Check for updates

THE AMERICAN SOCIETY OF MECHANICAL ENGINEERS
345 E. 47th St., New York, N.Y. 10017

97-GT-79

The Society shall not be responsible for statements or opinions advanced in papers or discussion at meetings of the Society or of its Divisions or Sections, or printed in its publications. Discussion is printed only if the paper is published in an ASME Journal. Authorization to photocopy material for internal or personal use under circumstance not falling within the fair use provisions of the Copyright Act is granted by ASME to libraries and other users registered with the Copyright Clearance Center (CCC) Transactional Reporting Service provided that the base fee of $0.30 per page is paid directly to the CCC, 27 Congress Street, Salem MA 01970. Requests for special permission or bulk reproduction should be addressed to the ASME Technical Publishing Department.

Copyright © 1997 by ASME All Rights Reserved Printed in U.S.A

AN OVERALL CORRELATION OF FILM COOLING EFFECTIVENESS FROM ONE ROW OF HOLES

S. Baldauf, A. Schulz, S. Wittig
Institut für Thermische Strömungsmaschinen
Universität Karlsruhe, Germany

Michael Scheurlen
Siemens AG/KWU
Mülheim/Ruhr, Germany

Downloaded from http://asmedigitalcollection.asme.org/GT/proceedings-pdf/GT1997/78705/V003T09A010/2410417/v003t09a010-97-gt-079.pdf by guest on 07 July 2022

ABSTRACT

Film cooling effectiveness of a single row of cylindrical holes on a flat plate was analyzed. It was found, that the flow can be divided into two typical regimes along the downstream distance. Near the ejection location a complex flow domain of cooling film formation with strong 3-D character was recognized. Further downstream a domain of a diluting cooling film with 2-D character was identified. An analytical solution for the film cooling effectiveness along the downstream distance was derived in the 2-D regime. Based on literature data, correlations for the formation length, i.e. the length of the 3-D domain, and the corresponding film cooling effectiveness at the start of the 2-D film were developed. These correlations provide the initial conditions of the analytical solution of the 2-D film flow. A damping function was introduced to connect the two regimes and to model the lateral averaged film cooling effectiveness distribution within the 3-D flow domain. From this, a correlation was established, taking into account the full set of parameters, which was presented in an earlier study [1]. The correlation was tested over a wide range of parameters, and an error estimation is given to demonstrate the quality of the correlation.

INTRODUCTION

Film cooling by compressor air through rows of holes is the most used external cooling technique in regions of highest thermal loads. The idea of film cooling is to establish a homogeneous, two dimensional film of coolant on the surface to be protected. Usually, the resulting heat flux problem is treated as two independent problems of temperature and heat transfer. These partial problems are characterized by the dimensionless temperature of the adiabatic wall

$$\eta = \frac{T_{AW} - T_G}{T_C - T_G} \qquad (1)$$

denoted film cooling effectiveness, and the heat transfer coefficient

$$h = \frac{q}{T_{AW} - T_W} \qquad (2)$$

Since the application of film cooling by rows of holes induces a highly complex boundary layer, even the prediction of the cooling effectiveness alone is difficult. The large number of influencing parameters precluded the generation of correlations or computations applicable to all cases, even for the flat plate film cooling by one row of inclined holes. As an earlier study of Baldauf and Scheurlen [1] showed, a complete collection of these parameters could not be found in the literature. As a result of that study this set of parameters was derived and lateral averaged effectiveness was demonstrated to result in

$$\bar{\eta} = f\left(M, I, Tu, \frac{x}{D}, \alpha, \frac{s}{D}, \frac{L}{D}, \frac{\delta_1}{D}\right) \qquad (3)$$

The set comprises the fluid dynamic parameters blowing ratio, momentum ratio, and turbulence intensity of the hot gas flow, and the geometrical parameters downstream distance, blowing angle, hole spacing, hole length, and thickness of the approaching boundary layer. Particularly, correlations for discrete hole film cooling accounting for the influences of boundary layer thickness, hole length, and turbulence could not be found. In the following a correlation system is presented that includes all the parameters indicated above and that exploits a large database offering a substantial variation of all these parameters.

INTENTION OF THE STUDY

The still intensive actual research indicates, that reliable tools for the prediction of film cooling performance of arbitrary configurations are not yet available. Computational fluid dynamics still suffer from inadequate flow discretisation and turbulence modeling. Carefully built computation models with refined calculation grids provide insight into flow phenomena and mixing processes, but the full complexity of the problem is not resolved [8]. For cooling optimization in iterative processes, these methods of computational fluid dynamics are too time consuming and, therefore, only useful in detail examinations. Correlations do not attempt to resolve the full complexity of the problem, but they systematically describe symptoms that result from the complex

Presented at the International Gas Turbine & Aeroengine Congress & Exhibition
Orlando, Florida — June 2–June 5, 1997

process. Known correlations for lateral averaged film cooling effectiveness reveal good results, if the configurations considered are not too far from the experimental conditions of the correlation's data base.

In integral computerized optimization of film cooled turbine parts fast and handy real time prediction methods are required. They have to be mostly independent of special boundary conditions and enable the systematic study of parameter variations. The knowledge of the entire set of parameters suggests the development of a new correlation for discrete hole film cooling. For the first time the interaction of all parameters can be regarded. Furthermore, it is intended to achieve a great flexibility by dividing the problem into independent models for particular mechanisms. Such a modular tool allows the inclusion of actual research results and extensions to more general applications.

ANALYSIS OF THE FILM COOLING PROCESS

The examined film cooling problem is the ejection from one row of cylindrical, streamwise inclined holes on a flat plate with zero pressure gradient. No specific cross flow at the hole entrance or hole geometry variation is regarded, since these variations can influence the coolant jet flow significantly [9, 22]. Considering the 3-D problem of discrete hole film cooling there is no closed film initially present from the ejection. In contrast to the 2-D case of continuous slot film cooling, the coolant emerges from the holes as single jets. With downstream convection of the jets, uncooled space between the holes is covered by the coolant due to turbulent mixing of the jets with the hot gas. The surface between the holes at the ejection location is externally uncooled and, as a consequence, film cooling effectiveness equals zero. With successive spreading of the jets, lateral averaged cooling effectiveness

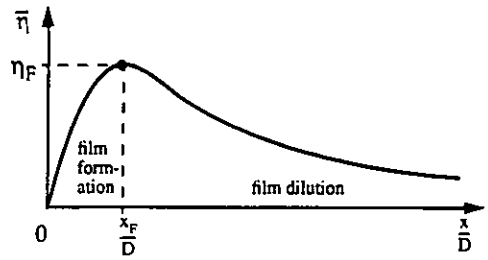

Figure 1: Lateral averaged effectiveness over downstream distance

rises towards a maximum as sketched in Figure 1. The maximum occurs near the point, where the coolant first forms a closed film over the surface. Once such a wall film with 2-D character is formed, it can be treated as a boundary layer like flow with specific temperature and velocity profiles. With increasing downstream distance, the velocity profiles transform into typical turbulent boundary layer profiles while the temperature distribution corresponds to a 2-D half-jet profile [7,23].

L'Ecuyer and Soechting [12] characterized three different regimes of the coolant jet mixing process with increasing velocity ratio, as indicated in Figure 2. In the mass addition regime, the coolant is squeezed between the hot gas flow and the wall. The high shear of the boundary layer causes the jets to spread out quickly and merge with adjacent jets. As long as this mixing scheme is present, an increase in the velocity ratio results in a higher coolant mass flux, forming a thicker film with higher thermal capacity and higher effectiveness at the point of film formation. In the mixing regime, the normal momentum of the coolant flow from inclined holes tends to drive the coolant away from the wall.

NOMENCLATURE

A	velocity profile parameter
a	correlation coefficients
α	blowing angle
b	correlation coefficients
C	coolant to hot gas thermal capacity ratio
c	correlation coefficients
c_p	thermal capacity at constant pressure, [J/(kg K)]
χ	ratio of shear layer to thermal layer thickness, δ_u/δ_τ
D	ejection hole diameter, [m]
d	correlation coefficients
δ	boundary layer thickness, [m]
δ_1	displacement thickness of the shear layer, [m]
f_d	damping function on the analytic effectiveness
G	relative cooling film thickness
h	heat transfer coefficient, [W/m^2 K)]
η	film cooling effectiveness
φ	correlation factors
I	coolant to hot gas momentum flux ratio, $(\rho u^2)_C/(\rho u^2)_G$
L	ejection hole length, [m]
λ	ratio of film mean temperature to adiabatic wall temperature
M	blowing ratio, $(\rho u)_C/(\rho u)_G$
m	gradient of thermal capacity ratio with density ratio
$\dot{m}$	mass flux, [kg/s]
n	velocity profile coefficient
p	pressure, [N/m^2]
q	heat flux, [W/m^2]
R	specific gas constant, [J/(kg K)]
Re	Reynolds number
P	coolant to hot gas density ratio, ρ_C/ρ_G
r	temperature ratio factor
s	ejection hole spacing, [m]
s_e	equivalent slot width, $s_e = \frac{\pi}{4} d \left(\frac{s}{d}\right)^{-t}$
σ	standard deviation
T	temperature, [K]
Tu	turbulence intensity, $\sqrt{\overline{u'^2}} / u$
U	coolant to hot gas velocity ratio, u_C/ u_G
u	velocity, [m/s]
v	film thickness ratio
x	downstream distance from hole center, [m]
y	coordinate normal to the wall, [m]

Subscripts

A	analytically derived
AW	adiabatic wall
C	coolant
D	hole diameter based
e	entrained
F	at film formation
f	cooling film
G	hot gas
λ	from temperature ratio integration
m	from mass flux integration
max	at maximum peak effectiveness
T	temperature layer
τ	integral temperature layer
u	shear layer
W	wall

Downloaded from http://asmedigitalcollection.asme.org/GT/proceedings-pdf/GT1997/78705/V003T09A010/2410417/v003t09a010-97-gt-079.pdf by guest on 07 July 2022

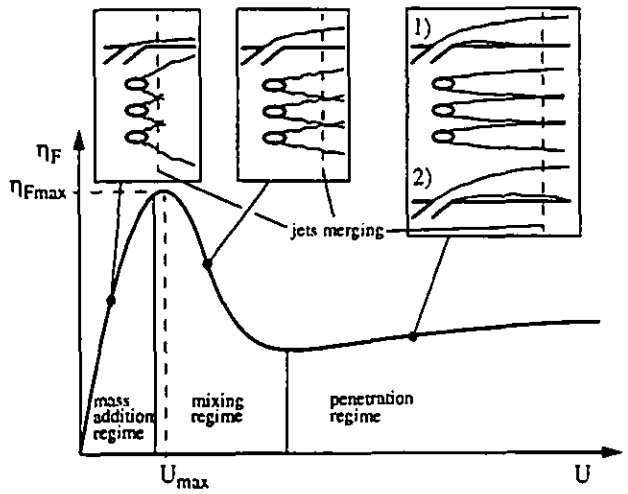

Figure 2: Maximum effectiveness η_F of film formation

The outer proportions of still attached jets begin to mix with the hot gas flow. A maximum of η_F is reached at the velocity ratio U_{max} before the mixing affects a significant fraction of the coolant. The following decay indicates the formation of thicker and less intense films, as large amounts of hot gas are entrained. With the increase of the coolant velocity, the maximum moves farther downstream before the spreading jets can merge. In the penetration regime, the high normal momentum of the coolant causes total detachment of the jets. Spreading of the jets now takes place apart from the wall, and by turbulent mixing only, the coolant can reach the wall. Here two schemes are possible as sketched in Figure 2: First, jet spreading causes the single jets to contact the wall and the reattached jets merge afterwards, forming the film. Second, the spreading jets merge off the wall, and turbulent growth leads to a reattachment of the accrued layer. In both cases a pronounced downstream distance is necessary for the coolant to form the film.

ANALYTICAL SOLUTION FOR THE LOCAL EFFECTIVENESS

The 2-D film can be described by similar velocity and temperature profiles. Figure 3 shows such profiles, envisioning a typical power law contour for the velocity

$$u(y) = u_G \left(\frac{y}{\delta_u}\right)^{1/n} \tag{4}$$

and an exponential curve for the temperature profile, as proposed by Wieghardt [23] and confirmed by others [14, 15]

$$\frac{T(y) - T_G}{T_{AW} - T_G} = \exp\left(-\left[\Gamma\left(\frac{3+\frac{1}{n}}{2+\frac{1}{n}}\right)\frac{y}{\delta_\tau}\right]^{2+\frac{1}{n}}\right) \tag{5}$$

$\Gamma(z)$ denotes the Gamma function and δ_τ is given by

$$\delta_\tau = \int_0^\infty \frac{T(y) - T_G}{T_{AW} - T_G}\, dy \tag{6}$$

The cooling film thickness δ_T can be defined at the wall distance, where 99% of the temperature difference from the wall to the free stream is passed through. Using a typical value of n=7, this is the case with

$$v_m = \frac{\delta_T}{\delta_\tau} = 2.3 \tag{7}$$

The mean temperature of the film can be found as a fraction of the

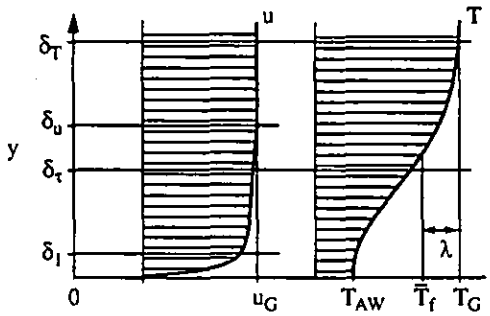

Figure 3: Velocity and temperature profiles of the cooling film

total temperature difference of the adiabatic wall to the hot gas:

$$\bar{T}_f - T_G = \lambda (T_{AW} - T_G) \tag{8}$$

This mean temperature results from the balance of mass and enthalpy of the growing cooling film (Figure 4). The cooling film can theoretically be traced back to an initial state of a uniform film of coolant with the cross sectional area of the ejection orifices used, resulting in an equivalent width of a tangential slot. Enthalpy flux of the film is given by the sum of coolant enthalpy and enthalpy of the entrained hot gas:

$$\overline{c_{pf}}\, \dot{m}_f\, \bar{T}_f = c_{pC}\, \dot{m}_C\, T_C + c_{pG}\, \dot{m}_e\, T_G \tag{9}$$

The average thermal capacity of the film $\overline{c_{pf}}$ results from the mixing of the mass flux of the initial coolant and the entrained hot gas

$$\overline{\rho u_f}\, \delta_T\, \overline{c_{pf}} = \dot{m}_C\, c_{pC} + (\dot{m}_f - \dot{m}_C)\, c_{pG} \tag{10}$$

The average mass flux of the film $\overline{\rho u_f}$ can be gained from the integration of velocity and density over the film height

$$\overline{\rho u_f} = \frac{1}{\delta_T} \cdot \int_0^{\delta_T} \rho\, u\, dy = \frac{p}{R\, \delta_T} \cdot \int_0^{\delta_T} \frac{u}{\bar{T}}\, dy \tag{11}$$

presuming ideal gases. There is no closed solution for this integration with the suggested profiles u(y) and T(y), although the result is known by numerical integration. The rules for the integration of continuous functions, however, specify that the density somewhere within the film must equal the required average value. Equation 11 then becomes

$$\overline{\rho u_f} = \frac{p(y^*)}{\delta_T} \cdot \left(\int_0^{\delta_\tau} u_G \left(\frac{y}{\delta_u}\right)^{\frac{1}{n}} dy + \int_{\delta_\tau}^{\delta_T} dy \right) \tag{12}$$

Assuming, that the wall distance y*, where the correct density is found, does not change substantially with temperature ratio, the film mass flux becomes

$$\overline{\rho u_f} = \frac{p_G}{r_m\left(\frac{T_{AW}}{T_G} - 1\right) + 1} \cdot \frac{u_G}{v_m}\left(v_m - \frac{\chi}{n+1}\right) \tag{13}$$

where χ is the ratio of δ_u on δ_τ. Factor r_m defines the fraction of the

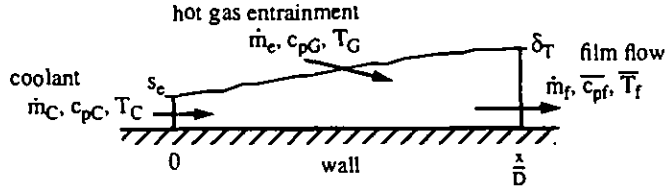

Figure 4: Control volume around the developing film

Downloaded from http://asmedigitalcollection.asme.org/GT/proceedings-pdf/GT1997/78705/V003T09A010/2410417/v003t09a010-97-gt-079.pdf by guest on 07 July 2022

temperature difference from the free stream to the wall that is passed through, when the average density is reached. r_m is found by comparison with the result of the numerical integration. Deviation of eq. 13 from the correct result is at most 1.4% within the relevant range of temperature ratios. Using eqs. 9-10, 13, the mean temperature of the film is

$$\frac{\bar{T}}{T_G} - 1 = \frac{\frac{T_C}{T_G} - 1}{1 + \frac{c_{pG}}{c_{pC}}\left(\frac{\rho_G u_G \delta_T}{\rho_C u_C s_e} \cdot \frac{v_m - \frac{\chi}{n+1}}{v_m r_m \left(\frac{T_{AW}}{T_G} - 1 \right) + v_m} - 1 \right)} \quad (14)$$

λ can be derived from the enthalpy weighted temperature profile:

$$\lambda = \frac{\int_0^{\delta_T} \frac{T - T_G}{T_{AW} - T_G} \rho u c_p \, dy}{\overline{\rho u_f} \; \overline{c_{pf}} \, \delta_T} \quad (15)$$

Expecting that c_p barely deviates from the mean value $\overline{c_{pf}}$ in the film, which is true for a developed film, the λ expression migrates to the mass weighted form. Here, too, no closed solution is available, but using the computed result expressions $\rho(y^*)$ and $u(y^*)$ can be found in an analogue procedure as used for the mass flux. First the mean velocity expression is determined to assure proper results at a density ratio of unity. The form of the velocity expression was chosen to be the same as resulting from the mass integration, so λ can be approximated by

$$\lambda = \frac{r_m \left(\frac{T_{AW}}{T_G} - 1 \right) + 1}{r_\lambda \left(\frac{T_{AW}}{T_G} - 1 \right) + 1} \cdot \frac{1}{v_\lambda} \frac{v_\lambda - \frac{\chi}{n+1}}{v_m - \frac{\chi}{n+1}} \quad (16)$$

Factor v_λ represents a fictitious ratio of integral temperature layer to film thickness to apply the same χ. Factor r_λ complements an appropriate fraction of the temperature difference. To achieve a handy form of the following equations, some dimensionless numbers are introduced:

$$A = v_m - \frac{\chi}{n+1} \qquad \text{velocity profile parameter} \quad (17)$$

$$G = \frac{\delta_T}{M s_e} \qquad \text{relative cooling film thickness} \quad (18)$$

$$C = \frac{c_{pC}}{c_{pG}} \approx 1 + m - mP \qquad \text{thermal capacity ratio} \quad (19)$$

Using air as coolant, eq. 19 gives a linear dependence of the thermal capacity ratio on the density ratio, since the temperature level and pressure of the domain do not influence this ratio significantly [1]. With a gradient of m=0.08 the deviation of the correlated C is at most 3% within the relevant range of density ratio. With help of eqs. 8, 14, 16-19, relative cooling film thickness turns into

$$G = \frac{C \, v_m \, v_\lambda}{A - v_m + v_\lambda} \left(\frac{1}{\eta_A} + r_\lambda \left(\frac{T_C}{T_G} - 1 \right) \right) - \frac{(C-1) \, v_m}{A} \left(1 + r_m \left(\frac{T_C}{T_G} - 1 \right) \eta_A \right) \quad (20)$$

with η_A denoting the film cooling effectiveness of the analytical film description. Solving eq. 20 for the effectiveness leads to a division by the factor $(C-1)$. This indicates a singularity for a density ratio of unity, which is physically not acceptable. Estimation of the last term in brackets in eq. 20 reveals, that all factors are of the order 10^{-1}. Thus, the resulting product is at least two orders of magnitude smaller then 1 and, therefore, negligible. Equation 20 can now be rewritten as

$$G = \frac{C \, v_m \, v_\lambda}{A - v_m + v_\lambda} \cdot \left(\frac{1}{\eta_A} + r_\lambda \left(\frac{T_C}{T_G} - 1 \right) \right) - \frac{(C-1) \, v_m}{A} \quad (21)$$

and film cooling effectiveness results in

$$\eta_A = \frac{1}{\frac{A - v_m + v_\lambda}{A} \cdot \left(\frac{GA}{C \, v_m \, v_\lambda} + \frac{(C-1)}{C} \cdot \frac{1}{v_\lambda} \right) - r_\lambda \left(\frac{T_C}{T_G} - 1 \right)} \quad (22)$$

COOLING FILM GROWTH WITH DOWNSTREAM DISTANCE

For the application of eq. 22, only the downstream development of film thickness δ_T and ratio of shear layer to temperature layer χ are required. As pointed out in the analysis, the flow of the 2-D film can be characterized by its shear layer, which is similar to a turbulent boundary layer, and its thermal layer, which shows half-jet behavior. The growth of turbulent jet width is linear with downstream distance [5, 19]. The dependence of the turbulent boundary layer growth on Reynolds number and downstream distance may be written as [19]

$$\frac{\delta_u}{D} = 0.37 \left(\frac{x}{D} \right)^{4/5} Re_D^{-1/5} \quad (23)$$

In the film cooling situation no developed and settled shear layers are present. There are pronounced disturbances, resulting from the ejection and enhancing the mixing processes. It is expected, therefore, that the growth of the shear layer over downstream distance will be faster, driving the exponent of x/D towards unity. Within the disturbed shear layers, the weak influence of Reynolds number will further decrease. This is supported by the result of the parameter study [1], showing no significant influence of hole Reynolds number on lateral averaged film cooling effectiveness.

The growth of both shear layer and temperature layer are governed by the same turbulent mixing processes, so the ratio of their thicknesses is expected to be constant. Several authors reported [17, 19, 21], that thermal layer growth reaches up to twice the shear layer growth, depending on the preferred orientation of the turbulent vortex structure. Since this preferred orientation may not be detected easily in the discussed film cooling problem, a constant ratio of 1.5 was chosen, resulting in a parameter χ=1.53. In fact, Mayle et al. [14] gave a value of 0.65 for the ratio of the thicknesses δ_T/δ_u for large downstream distances of a slot injection, resulting in a parameter χ=1.54. High turbulence levels tend to dilute the cooling film faster then low turbulence levels and, therefore, enhance the growth of the film layer. Small variations at low turbulence levels cause minor effects. With these assumptions, linear film growth from the point of film formation with the initial film thickness δ_{TF} and an exponential effect of turbulence, chosen for simplicity reasons, can be expressed as

$$\frac{\delta_T}{D} = a_1 \left(\frac{x}{D} - \frac{x_F}{D} \right) \exp(a_2 Tu) + \frac{\delta_{TF}}{D} \quad (24)$$

CORRELATION OF FILM FORMATION LENGTH

As discussed in the analysis, the starting conditions of the film have to be correlated from experimental data. Influences of all given parameters have to be described in a general form of a correlation equation, and adjustable coefficients for the correct weighting of the parameters have to be applied.Experimental data of lateral averaged adiabatic effectiveness or impermeable wall effectiveness in mass transfer experiments, respectively, of flat plate test cases were taken from literature

Downloaded from http://asmedigitalcollection.asme.org/GT/proceedings-pdf/GT1997/78705/V003T09A010/2410417/v003t09a010-97-gt-079.pdf by guest on 07 July 2022

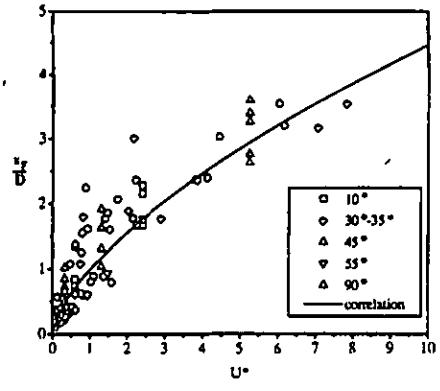

Figure 5: Correlation of x_F/D

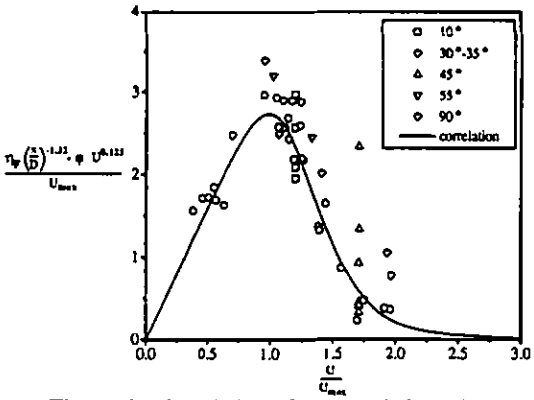

Figure 6a: Correlation of η_F, mass/mix regimes

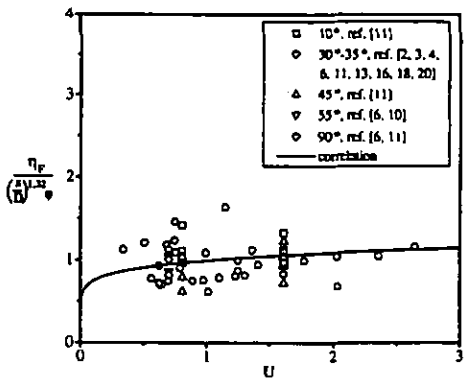

Figure 6b: Correlation of η_F, penetration regime

[2, 3, 4, 6, 10, 11, 13, 16, 18, 20], to derive the coefficients in least squares fits. The parameter ranges of these data are given in Table 1.

A closed film will start directly at the ejection location in the case of continuous slot ejection. The „distance" of holes that have an equivalent slot width of one diameter is $s=\pi D/4$. Therefore, dependence of formation length on the hole spacing is formed by

$$\frac{x_F}{D} = f\left(\frac{s}{D}-\frac{\pi}{4}\right)^{b_2} \tag{25}$$

Influence of hole length, approaching boundary layer thickness, and hot gas turbulence result in earlier or later formation of the film. Power laws are adopted for boundary layer thickness and hole length, excluding zero values. Since turbulence values near zero in experiments are often found, the power law is not useful and an exponential law was chosen. With an angle and velocity ratio dependent term U* the complete correlation equation then becomes

$$\frac{x_F}{D} = b_1\left(\frac{s}{D}-\frac{\pi}{4}\right)^{b_2} U^{*b_3}\left(\frac{L}{D}\right)^{b_4}\left(\frac{\delta_1}{D}\right)^{b_5}\exp\left(b_6\,Tu\right) \tag{26}$$

The development of the expression U* is based on the assumption that formation length should depend on the downstream velocity component of the coolant. For steep blowing angles the film forms close to the ejection location, because of a small initial downstream velocity component of the coolant and intense turbulent mixing. In case of shallow angles, large downstream velocity components tend to drive the coolant far downstream before film formation takes place. From the experimental data, however, can be seen, that very shallow angles also result in quite small formation lengths. This may be caused by the high shear gradients close to the wall. A simple function describing this behavior with the ejection angle is $\sin^2(2\alpha)$. A density ratio dependence of U* was considered in form of a power law. The least squares fit revealed, that the proper combination of velocity ratio and density ratio in U* is the momentum ratio. At last, tangential ejection of single jets also needs some downstream distance to form a film. Adopting this idea of an angle independent part of U*, it was formed as

$$U^* = I\left(b_7 + \sin^2(2\alpha)\right) \tag{27}$$

All coefficients resulting from the least squares fit are listed in Table 1. Scattering of the data around the curve given by eq. 26 is envisioned in Figure 5. Standard deviation of film formation lengths taken from experimental measurements from the calculated values is

$$\sigma_{\frac{x_F}{D}} = RMS\left(\Delta\frac{x_F}{D}\right) = 3.37 \tag{28}$$

This seems to be a high value as observable from the width of the scatter band in Figure 5.Determination of the location of peak effectiveness is an interpretation of the experimental data and especially in cases of large formation lengths large errors occur. Considering, that this RMS value includes formation lengths up to 60 D, the value is acceptable.

CORRELATION OF THE PEAK EFFECTIVENESS

A description of the general behavior of peak effectiveness over velocity ratio (see Figure 2) is given by an equation of the form

$$\eta_F = \left(\varphi\,U^{c_1} + \frac{c_4 U}{\frac{1}{c_2-1}\left(\frac{U}{U_{max}}\right)^{c_2}+1}\right)\cdot\left(\frac{s}{D}\right)^{c_3} \tag{29}$$

The first term describes the peak effectiveness within the penetration regime, the second an overshoot of the peak effectiveness in the mass addition and mixing regimes. The hole spacing is expected to have a general effect on the peak effectiveness. Factor φ includes the dependence on blowing angle, density ratio, hole length, thickness of the boundary layer and turbulence intensity within the penetration regime. The data available for angle variations suggest only a slight decrease for large angles, while there seems to be a substantial increase for very small angles. Modeling the other influences in the same way as for the formation length, factor φ was chosen to be

$$\varphi = c_{11}\left(c_5 - \sin^{c_6}\alpha\right)P^{c_7}\left(\frac{L}{D}\right)^{c_8}\left(\frac{\delta_1}{D}\right)^{c_9}\exp\left(c_{10}Tu\right) \tag{30}$$

U_{max} is governed by the normal momentum of the coolant, depending directly on the blowing angle. The critical normal momentum at maximum peak effectiveness also is influenced by hole length, thickness of approaching boundary layer, turbulence intensity of the hot gas flow and hole spacing. An angle independent part of U_{max} is applied, because an infinite maximum peak effectiveness for tangential ejection is not reasonable. With these assumptions, U_{max} becomes

$$U_{max} = \frac{\sqrt{\frac{c_{16}}{P}\left(\frac{L}{D}\right)^{c_{12}}\left(\frac{\delta_1}{D}\right)^{c_{13}}\exp\left(c_{14}Tu\right)\left(\frac{s}{D}\right)^{c_{17}}}}{c_{15}+\sin\alpha} \tag{31}$$

In the least squares fit, exponent c_1 did not result in stable values. A fit of the data high in the penetration regime revealed a value of 0.125, what seemed to be acceptable for all data and, therefore, was set constant in the further fitting process. Coefficient c_{15} of the angle independent part of U_{max} tended towards large values, „choking" the angle dependence of U_{max}. Since there is a significant difference of U_{max} by

Downloaded from http://asmedigitalcollection.asme.org/GT/proceedings-pdf/GT1997/78705/V003T09A010/2410417/v003t09a010-97-gt-079.pdf by guest on 07 July 2022

normal blowing versus blowing at shallow angles, c_{15} was limited to a maximum value of 3, leading to a plausible variation with blowing angle and good results of the fit. Exponent c_{17} of the hole spacing dependence of U_{max} was expected to be negative, since interaction of jets from holes with small spacing should result in better deflection of the coolant. c_{17} did not move to negaive values, so the influence of hole spacing was removed.

The coefficient values resulting from the least squares fit are summarized in Table 1. Scattering of the measured data around the correlation curve is given in Figure 6a for the overshoot within the mass addition and mixing regimes and in Figure 6b for the penetration regime. Standard deviation of the measured data from the fit curve is

$$\sigma_{\eta_F} = RMS(\Delta\eta_F) = 0.031 \qquad (32)$$

This value is good and gives confidence in the correlation equations used. It turned out to be much easier to read peak effectiveness values from the experimental data than the film formation lengths. The scatter at the beginning of the penetration regime in Figure 6b, however, documents that the flow situation is highly sensitive to small variations at transition from the mixing to the penetration regime.

COUPLING OF CORRELATION AND ANALYTICS

Within the film formation region, lateral averaged effectiveness typically composes of low values in the midlines between the holes and high values in the hole center lines. Low average cooling effectiveness can be seen as a fraction of the possible effectiveness in the presence of an ideal cooling film. Following this, a fictive 2-D film can be calculated backwards from the point of film formation into the formation region (Figure 7). Lateral averaged effectiveness can then be described by a damping function, modeling the continuous approach of the actual effectiveness towards ideal analytic effectiveness

$$\bar{\eta} = f_d \eta_A = \left(1 - (1 - f_{dF})^{\frac{x}{x_F}}\right)\eta_A \qquad (33)$$

where

$$f_{dF} = d_1 \exp\left(-d_2 \frac{x_F}{D}\right) \qquad (34)$$

Coefficients d_1 and d_2 were determined from the experimental data in a least squares fit together with coefficients a_1 and a_2 of the film development in eq. 24. Difficulties arose concerning parameter d_1, since a tendency towards values beyond one was observed. Data indicate, that there should be a formation length independent part of f_{dF} with a value close to one, so d_1 was set to 0.99. The other coefficients resulting from the fit and the complete correlation system are shown in Table 1. Standard deviation of experimental curves of effectiveness over downstream distance versus correlated curves is

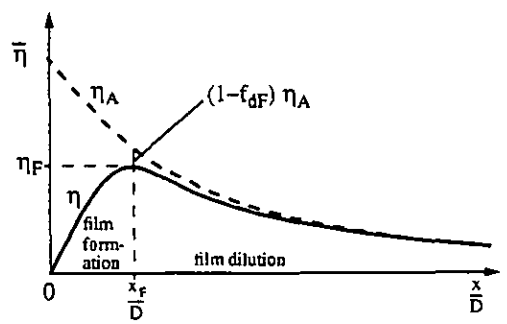

Figure 7: Damping function on analytic effectiveness

Formation length

$$\frac{x_F}{D} = b_1\left(\frac{s}{D} - \frac{\pi}{4}\right)^{b_2} U^{*b_3}\left(\frac{L}{D}\right)^{b_4}\left(\frac{\delta_1}{D}\right)^{b_5}\exp(b_6\,Tu)$$

$$U^* = 1\left(b_7 + \sin^2(2\alpha)\right)$$

b_1	b_2	b_3	b_4	b_5	b_6	b_7
1.8	1	0.65	0.323	-0.285	-9.32	0.631

Peak effectiveness

$$\eta_F = \left(\varphi U^{c_1} + \frac{c_4 U}{\frac{1}{c_2 - 1}\left(\frac{U}{U_{max}}\right)^{c_2} + 1}\right)\cdot\left(\frac{s}{D}\right)^{c_3}$$

$$\varphi = c_{11}\left(c_5 - \sin^{c_6}\alpha\right)P^{c_7}\left(\frac{L}{D}\right)^{c_8}\left(\frac{\delta_1}{D}\right)^{c_9}\exp(c_{10}Tu)$$

$$U_{max} = \frac{\sqrt[4]{\frac{c_{16}}{P}\left(\frac{L}{D}\right)^{c_{12}}\left(\frac{\delta_1}{D}\right)^{c_{13}}\exp(c_{14}Tu)}}{c_{15} + \sin\alpha}$$

c_1	c_2	c_3	c_4
0.125	7.6	-1.32	3.17
c_5	c_6	c_7	c_8
1.0253	0.012	0.74	-0.1
c_9	c_{10}	c_{11}	c_{12}
0.151	3.49	27.7	0.28
c_{13}	c_{14}	c_{15}	c_{16}
-0.57	-11.3	3	0.295

Film thickness at film formation

$$G_F = \frac{C\,v_m\,v_\lambda}{A - v_m + v_\lambda}\cdot\left(\frac{f_{dF}}{\eta_F} + r_\lambda\left(\frac{1}{P} - 1\right)\right) - \frac{(C-1)\,v_m}{A} \qquad A = v_m - \frac{\chi}{n+1} \qquad C = 1 + m - mP$$

$$f_{dF} = d_1\exp\left(-d_2\frac{x_F}{D}\right)$$

v_m	v_λ	r_λ	χ	n	m	d_1	d_2
2.3	1.17	0.71	1.53	7	0.07	0.99	0.0023

Filmgrowth with downstream length

$$\frac{\delta_T}{D} = a_1\left(\frac{x}{D} - \frac{x_F}{D}\right)\exp(a_2 Tu) + \frac{\delta_{TF}}{D} \qquad \frac{\delta_{TF}}{D} = \frac{G_F\,M\,\pi}{4\,\frac{s}{D}}$$

a_1	a_2
0.04	9.53

Effectiveness with downstream length

$$\bar{\eta} = \frac{f_d}{\frac{A - v_m + v_\lambda}{A}\cdot\left(\frac{GA}{C\,v_m\,v_\lambda} + \frac{(C-1)}{C}\cdot\frac{1}{v_\lambda}\right) - r_\lambda\left(\frac{1}{P} - 1\right)} \qquad f_d = 1 - (1 - f_{dF})^{\frac{x}{x_F}} \qquad G = \frac{4}{M\pi}\,\frac{s}{D}\,\frac{\delta_T}{D}$$

Parameter range

M	P	Tu	$\frac{s}{D}$	α	$\frac{L}{D}$	$\frac{\delta_1}{D}$
0.16 ... 2	0.76 ... 2	0 ... 0.17	$\frac{\pi}{4}$ ... 5	10°... 90°	1.5 ... 20	0.06 ... 0.17

Table 1: The correlation system and its coefficients

$$\sigma_\eta = RMS(\Delta\eta) = 0.033 \qquad (35)$$

giving confidence in the presented correlation system.

PARAMETER VARIATION STUDY ON THE CORRELATION

To visualize the effects of the influencing parameters, a variation around a working point is presented. The working point chosen is a typical experimental setup, often used as a reference case in the effectiveness measurements. The parameters of this working point are listed in Table 2 and effects of parameter variations are discussed for the three regimes.

The extensions of the regimes emerge by a variation of the blowing ratio as shown in Figure 8. At M=0.3 the typical mass addition regime distribution can be seen, with a sharp and early peek of effectiveness and a following fast decay. Increasing the blowing ratio increases the peak effectiveness and gradually enlarges the film formation length. Blowing ratio of maximum peak effectiveness strongly depends on the density ratio and is about M=0.5 for the present conditions. For low density ratios of P=1 the maximum occurs around M=0.4, for high density ratios of P=2 it can be observed at about M=0.55. Further increasing the blowing ratio decreases peak effective-

$\frac{s}{D}$	P	α	$\frac{L}{D}$	$\frac{\delta_1}{D}$	Tu
3	1.5	35°	10	0.1	0.02

Table 2: Working point for the parameter variation

Downloaded from http://asmedigitalcollection.asme.org/GT/proceedings-pdf/GT1997/78705/V003T09A010/2410417/v003t09a010-97-gt-079.pdf by guest on 07 July 2022

ness, while the peak location moves downstream and the decay becomes less steep. No significant effect on effectiveness can be seen far downstream and an optimum coolant use at $U=U_{max}$ is clearly indicated. A minimum of peak effectiveness occurs near M=1, marking the end of the mixing regime and total jet detachment under present conditions. In the penetration regime, increasing the blowing ratio gradually augments the peak effectiveness and substantially enlarges the film formation length. Effectiveness decay after the peak is very slow.

Variation of the hole spacing (Figure 9a):

The effectiveness decreases monotonically with increasing hole spacing, while the peak moves downstream. The only way to get high effectiveness by use of high blowing ratios in the penetration regime is a very small hole spacing, leading to an early mixing of the coolant jet and formation of a thick and intense film that dilutes only slowly.

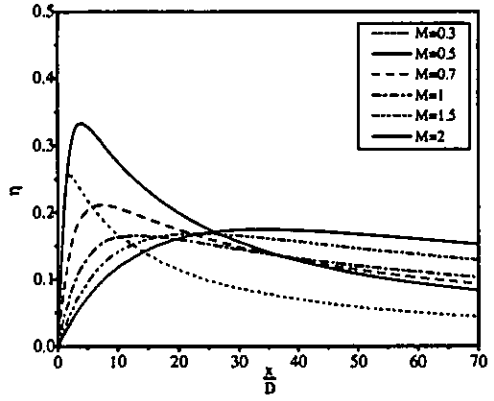

Figure 8: Effectiveness over down stream distance in different regimes

Variation of the density ratio (Figure 9b):

In the mass addition regime density ratio influence is weak. A lower density ratio is superior here, because it yields an approach of the coolant velocity towards the hot gas velocity. In the mixing regime a wide spreading of the curves can be seen. Low density ratio causes a higher jet momentum, driving the coolant away from the wall. In the penetration regime also the clear advantage of high density ratios is obvious.

Variation of the blowing angle (Figure 9c):

In the mass addition regime a benefit from small blowing angles can be seen, but the effect on downstream effectiveness is weak. In the mixing regime the advantage for the small angles becomes very pronounced, when higher normal momentum causes the jets from large angle holes to mix up in the hot gas. Film formation length is largest for the medium angles and decreases for both large and small angles. In the penetration regime small angles are also superior and the shorter formation length for small angles additionally rise overall effectiveness.

Variation of hole length (Figure 9d):

In the mass addition regime no significant effect can be seen. As soon as the mixing regime is reached the curves spread out. The velocity profile distorted by secondary flows at the exit of a short hole has a higher effective momentum driving the coolant off the wall than a developed pipe flow of a long hole. At the end of the mixing regime the curves collapse. In the penetration regime short holes are advantageous. The shorter formation length for short holes results in higher effectiveness near the ejection, but downstream no effect is visible.

Variation of the boundary layer thickness (Figure 9e):

Again no significant effect can be detected in the mass addition regime. In the mixing regime a thin approaching boundary layer leads to a considerably better peak effectiveness because of intense jet deflection by

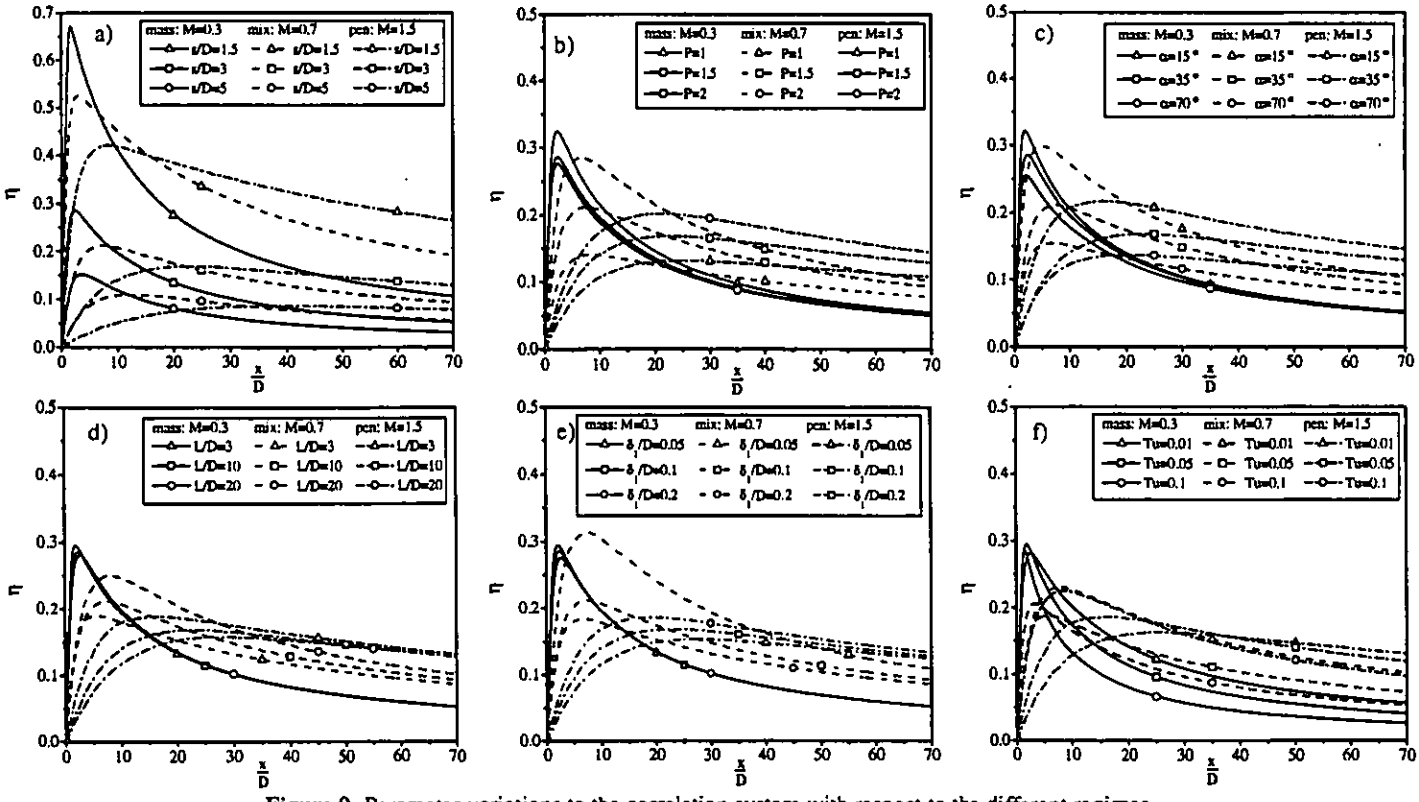

Figure 9: Parameter variations to the correlation system with respect to the different regimes

Downloaded from http://asmedigitalcollection.asme.org/GT/proceedings-pdf/GT1997/78705/V003T09A010/2410417/v003t09a010-97-gt-079.pdf by guest on 07 July 2022

the hot gas stream. Similar to the hole length variation, a contraction of the curves at the end of the mixing regime takes place. In the penetration regime higher effectiveness is reached with thick boundary layers because of faster jet spreading in the delayed wall region.

Variation of the turbulence intensity (Figure 9f):
In the mass addition regime, the films for high turbulence intensities dilute much faster than for low ones. In the mixing regime significantly shorter film formation lengths are present for high turbulence intensities, but the low intensity value leads to a higher and broader peak with a following slower decay of effectiveness. With high turbulence intensities the curves of the penetration regime begin to mix up with those of the mixing regime. Short formation lengths for high turbulence levels here lead to relatively early peaks with a following fast decay. Only very close to the ejection location this results in higher effectiveness, farther downstream low turbulence always is advantageous.

CONCLUSIONS

A new correlation for adiabatic film cooling effectiveness by coolant ejection from one row of holes is presented. For first time this correlation includes the full set of influencing parameters and their interaction on this problem. As can be seen from the discussion of the error values, the correlation describes the measured data with good accuracy and confidence. The modular structure of the system allows extensions to the correlation models to include parameters of more general cases, involving wall curvature or pressure gradients.

Examination of the available data within the development process of the correlation models revealed, that there are still gaps in the database. Particularly systematic variations of the blowing angle with respect to the different regimes are necessary.

Most important aim of this work was the creation of a tool, that enables the prediction of the systematic effects of all relevant parameters. The presented parameter variation study demonstrates that the influences from the seldom examined parameters of hole length, boundary layer thickness and turbulence intensity are of the same order as those of more commonly investigated parameters like density ratio and blowing angle.

REFERENCES

[1] Baldauf, S., Scheurlen, M., „CFD Based Sensitivity Study of Flow Parameters for Engine Like Film Cooling Conditions", ASME Paper 96-GT-310, 1996

[2] Barlow, D. N., Kim, Y. W., „Effect on Surface Roughness on Local Heat Transfer and Film Cooling Effectiveness", ASME Paper 95-GT-14, 1995

[3] Bons, J. P., MacArthur, C. D., Rivir, R. B., „The Effect of High Free Stream Turbulence on Film Cooling Effectiveness", ASME Paper 94-GT-51, 1994

[4] Ekkad, S. V., Zapata, D., Han, J.-C., „Film Effectiveness Over a Flat Surface With Air and CO_2 Injection Through Compound Angle Holes Using a Transient Liquid Crystal Image Method", ASME Paper 95-GT-11, 1995

[5] Eskinazi, S., Kruka, V., „Mixing of a Turbulent Wall Jet into a Free-Stream", Journal of Engineering Mechanics Division, ASME Proceedings, vol. 88, pp. 125-143, 1962

[6] Foster, N. W., Lampard, D., „The Flow and Film Cooling Effectiveness Following Injection Through a Row of Holes", Journal of Engineering for Power, vol. 102, pp. 584-588, 1980

[7] Goldstein, R. J.,"Film Cooling", Advances in Heat Transfer, vol. 7, Academic press, New York, pp. 321-379, 1971

[8] Giebert, G.; Gritsch, M., Schulz, A., Wittig, S., „Film-Cooling from Holes With Expanded Exits: A Comparison of computational Results With Experiments", Accepted for presentation at the 42nd Annual International Gas Turbine and Aeroengine Congress and Exposition, Orlando, Florida, USA, June 2-5, 1997

[9] Gritsch, M., Schulz, A., Wittig, S., „Adiabatic Wall Effectiveness Measurements for Film-Cooling Holes with Expanded Exits", Accepted for presentation at the 42nd Annual International Gas Turbine and Aeroengine Congress and Exposition, Orlando, Florida, USA, June 2-5, 1997

[10] Kohli, A., Bogard, D. G., „Adiabatic Effectiveness, Thermal Fields, and Velocity Fields for Film Cooling With Large Angle Injection", ASME Paper 95-GT-219, 1995

[11] Kruse, H., „Effects of Hole Geometry, Wall Curvature and Pressure Gradient on Film Cooling Downstream of a Single Row", AGARD-CP-390, pp. 8.1-8.13, 1985

[12] L'Ecuyer, M. R., Soechting, F. O., „A Model for Correlating Flat Plate Film Cooling Effectiveness for Rows of Round Holes", AGARD-CP-390, pp 19.1-19.12, 1985

[13] Liess, C., „Experimental Investigation of Film-Cooling With Injection from a Row of Holes for the Application to Gas Turbine Blades", Journal of Engineering for Power, vol.97, pp. 21-27, 1975

[14] Mayle, R. E., Kopper, F. C., Blair, M. F., Bailey, D. A., „Effect of Streamline Curvature on Film Cooling", Journal of Engineering for Power, vol. 99, no. 1, pp. 77-82, 1977

[15] Paradis, M. A., „Film Cooling of Gas Turbine Blades: A Study of the Effect of Large Temperature Differences on Film Cooling Effectiveness", Journal of Engineering for Power, vol. 99, no. 1, pp. 11-20, 1977

[16] Pedersen, D. R., Eckert, E. R. G., Goldstein, R. J., „Film Cooling With Large Density Differences Between the Main Stream and the Secondary Fluid Measured by the Heat-Mass Transfer Analogy", Journal of Heat Transfer, vol. 99, pp. 620-627, 1977

[17] Reichardt, H., „Impuls und Wärmeaustausch in freier Turbulenz", ZAMM 21, s. 257, 1941

[18] Remmlinger, U., „Die Vorhersage der Kühlwirkung bei Gasturbinenschaufeln aus Messungen in einem Heißwindkanal mit Triebwerksähnlichkeit unter Berücksichtigung des Einflusses variabler Stoffwerte", Dissertation, Technische Hochschule Darmstadt, 1988

[19] Schlichting, H., Riegels, F. W., „Grenzschichttheorie", 8. Auflage, Braun-Verlag, Karlsruhe, 1982

[20] Sinha, A. K., Bogard, D. G., Crawford, M. E., „Film Cooling Effectiveness Downstream of a Single Row of Holes With Variable Density Ratio", Journal of Turbomachinery,vol. 113, pp. 442-449, 1991

[21] Taylor, G. I., „The Transport of Vorticity and Heat Through Fluids in Turbulent Motion", Appendix by A. Fage, and V. M. Falkner, Proceedings of the Royal Society A 135, 685-705, 1932

[22] Thole, K. A., Gritsch, M., Schulz, A., Wittig, S., „Effect of a Crossflow at the Entrance to a Film-Cooling Hole", Accepted for Publication in the ASME Journal of Fluids Engineering

[23] Wieghardt, K., „Hot-Air Discharge for De-Icing", AAF Translation No. F-TS919-RE, Air Material Command, 1946

Downloaded from http://asmedigitalcollection.asme.org/GT/proceedings-pdf/GT1997/78705/V003T09A010/2410417/v003t09a010-97-gt-079.pdf by guest on 07 July 2022